Nuclear Materials and Energy 12 (2017) 60–74

Contents lists available at ScienceDirect

Nuclear Materials and Energy

journal homepage: www.elsevier.com/locate/nme

Physics conclusions in support of ITER W divertor monoblock shaping

R.A. Pitts[a,*], S. Bardin[b], B. Bazylev[c], M.A. van den Berg[b], P. Bunting[d], S. Carpentier-Chouchana[e], J.W. Coenen[f], Y. Corre[g], R. Dejarnac[h], F. Escourbiac[a], J. Gaspar[i], J.P. Gunn[g], T. Hirai[a], S-H. Hong[j], J. Horacek[h], D. Iglesias[d], M. Komm[h], K. Krieger[k], C. Lasnier[l], G.F. Matthews[d], T.W. Morgan[b], S. Panayotis[a], S. Pestchanyi[c], A. Podolnik[h], R.E. Nygren[m], D.L. Rudakov[n], G. De Temmerman[a], P. Vondracek[h], J.G. Watkins[m]

[a] ITER Organization, Route de Vinon-sur-Verdon, CS 90 046, 13067 St. Paul Lez Durance Cedex, France
[b] DIFFER-Dutch Institute for Fundamental Energy Research, De Zaale 20, 5612 AJ Eindhoven, The Netherlands
[c] KIT, Hermann-von-Helmholtz-Platz 1, Eggenstein-Leopoldshafen, Germany
[d] CCFE, Culham Science Centre, Abingdon, Oxon, OX14 3DB, UK
[e] EIRL SCC, F-13650 Meyrargues, France
[f] Forschungszentrum Jülich GmbH, Institut fuer Energie und Klimaforschung, Jülich, Germany
[g] CEA, IRFM, F-13108 Saint-Paul-Lez-Durance, France
[h] Institute of Plasma Physics, CAS v.v.i., Prague, Czech Republic
[i] IUSTI UMR 7343 CNRS, Aix-Marseille Université, 5 rue Enrico Fermi, 13453 Marseille, France
[j] National Fusion Research Institute, 169-148 Gwahangno, Yusung-Gu, Daejeon, Korea
[k] Max-Planck-Institut für Plasmaphysik, 85748 Garching, Germany
[l] Lawrence Livermore National Laboratory, 700 East Avenue, Livermore, CA 94551, USA
[m] Sandia National Laboratories, PO Box 5800, Albuquerque, NM 87185, USA
[n] University of California San Diego, 9500 Gilman Drive, La Jolla, CA, 92093-0417, USA

ARTICLE INFO

Article history:
Received 2 September 2016
Revised 14 February 2017
Accepted 6 March 2017
Available online 18 March 2017

Keywords:
ITER
Tungsten
Divertor
Shaping
Melting
MEMOS

ABSTRACT

The key remaining physics design issue for the ITER tungsten (W) divertor is the question of monoblock (MB) front surface shaping in the high heat flux target areas of the actively cooled targets. Engineering tolerance specifications impose a challenging maximum radial step between toroidally adjacent MBs of 0.3 mm. Assuming optical projection of the parallel heat loads, magnetic shadowing of these edges is required if quasi-steady state melting is to be avoided under certain conditions during burning plasma operation and transiently during edge localized mode (ELM) or disruption induced power loading. An experiment on JET in 2013 designed to investigate the consequences of transient W edge melting on ITER, found significant deficits in the edge power loads expected on the basis of simple geometric arguments, throwing doubt on the understanding of edge loading at glancing field line angles. As a result, a coordinated multi-experiment and simulation effort was initiated via the International Tokamak Physics Activity (ITPA) and through ITER contracts, aimed at improving the physics basis supporting a MB shaping decision from the point of view both of edge power loading and melt dynamics. This paper reports on the outcome of this activity, concluding first that the geometrical approximation for leading edge power loading on radially misaligned poloidal leading edges is indeed valid. On this basis, the behaviour of shaped and unshaped monoblock surfaces under stationary and transient loads, with and without melting, is compared in order to examine the consequences of melting, or power overload in context of the benefit, or not, of shaping. The paper concludes that MB top surface shaping is recommended to shadow poloidal gap edges in the high heat flux areas of the ITER divertor targets.

1. Introduction

The ITER tokamak divertor (Fig. 1) is the largest, most complex and most expensive component of this type ever constructed [1,2]. It is a fully water-cooled, tungsten (W) armoured unit, comprising

* Corresponding author.
E-mail address: richard.pitts@iter.org (R.A. Pitts).

http://dx.doi.org/10.1016/j.nme.2017.03.005

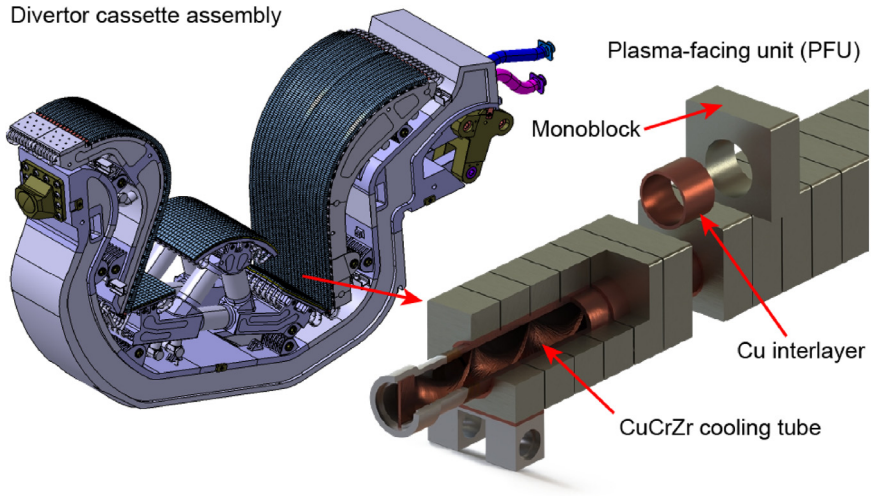

Fig. 1. CAD models of a single cassette of the 54 units in the ITER W divertor and exploded view of a portion of one of the PFUs bearing W monoblocks (note that this is not a precise representation of the actual MB design).

54 stainless steel cassettes bearing vertical targets, themselves constituted of a series of plasma-facing units (PFU) made up of chains of W monoblocks (MB) bonded to a CuCrZr cooling tube. These MB are rated for a stationary power handling capacity of $\sim$10 MW m^{-2}, with excursions (referred to as "slow transients") of twice this value (20 MW m^{-2}) for shorter time durations (several seconds) up to several hundred cycles. This capability was derived broadly from physics analysis (mostly based on SOLPS-4.3 plasma boundary code simulations, e.g. [3,4]), but is also determined to some extent by the limits of available technology. It is built into the engineering qualification imposed on the PFU suppliers, who must demonstrate integrity of the components for 5000 heat load cycles of 10 s duration at 10 MW m^{-2}, in addition to 300 cycles of 10 s at 20 MW m^{-2} (performed using electron beam facilities) [5,6]. These criteria are intended to provide a component capable of survival from the start of ITER operations through to the end of the first DT phase when the primary mission goal of long pulse (several hundred seconds, burning plasma operation at $Q_{DT} = 10$) will have been routinely achieved.

After several years of refinement following the decision in 2011 to discard the original strategy of a CFC/W target for non-active phase operations [2], the remaining key element of the ITER full W divertor design requiring consolidation is the issue of MB front surface shaping. The use of all-metal plasma-facing armour, especially in high heat flux (HHF) areas, imposes a design in which component melting is avoided if at all possible. Given the glancing angles at which magnetic field lines impact surfaces in tokamak divertors, this means avoiding leading edges (LE) which may occur due to tolerance build-up during manufacture and installation of components.

"Global" shaping, in the form of tilting of the entire vertical targets ($\sim$0.5°), protects the unavoidable gross misalignments (few mm) appearing between individual cassettes (see Fig. 2a), whilst specific shaping of selected MBs at the toroidal extremities of outer vertical target baffle area provides some mitigation against the intense transient heat fluxes expected during downward vertical displacement events [2,7,8]. On the vertical targets, engineering specifications require that the radial step, d between toroidally adjacent PFUs in the HHF areas not exceed a challenging d = 0.3 mm, for inter-PFU poloidal gaps of 0.5 mm (Fig. 2b). Thermal simulations (see Section 3.4) show that such (poloidal gap) edges will melt for parallel power flux densities $q_{||} \sim 250$ MW m^{-2}, corresponding to $\sim$15 MW m^{-2} on the top surface of an unshaped MB for the $\sim$3.5° field line angle of incidence in the baseline ($I_p = 15$ MA, $B_\varphi = 5.3$ T) ITER burning plasma equilibrium (taking into account the global target tilt). Such power fluxes are easily attainable on ITER in the event, for example, of uncontrolled divertor reattachment events. Melting of these MB LEs is also expected under transient heat fluxes due to ELMs or disruptions. In fact, the avoidance of edge melting (and hence the provision of a factor 2–3 against full surface melting) in the absence of misalignments (perfect MB alignment), is the origin of the specification on the maximum Type I ELM energy loss, ΔW_{ELM}, used to define the ITER ELM control requirements [2,9]. In this paper, LE disruption-induced heat loads will not be discussed further. With regard to fast transients, focus here will be on ELMs simply because many more such events are expected.

To protect inter-PFU MB radial misalignments, the baseline ITER divertor design solution is to include a simple toroidal bevel on the MB front surface (Fig. 2b). With bevel height of 0.5 mm over a toroidal extent of 28 mm (the standard dimension in the HHF area of the outer vertical target), the bevel angle of $\sim$1° adds to the global tilt and the field line incidence angle to define the total angle for projection of parallel power flux onto the top surface. Considerable effort has been invested in a physics and thermal response study of this simple MB shaping option subject to steady state and transient (ELM) ion fluxes, employing 3D ion orbit calculations [10,11], benchmarked against 2D particle-in-cell (PIC) modelling, the latter self-consistently including local electric fields [12]. The result is that although the solution does of course eliminate the poloidal edge melting issue for steady state loading, the increased angle between the surface and the field lines increases the top surface power flux density and reduces the margins both against ELM driven melting and the avoidance of surface temperatures (T_{surf}) in excess of W recrystallization for steady state power flux densities. In addition, toroidal bevelling does not eliminate the appearance of local hot spots due to particle penetration down gaps between MBs and ELM induced melting of toroidal gap edges [10,11].

The general issue of W leading edge loading in a real tokamak environment at ITER relevant (controlled) ELM energy flux densities was addressed by a dedicated experiment conducted on JET in 2013 [13,14]. A single lamella in one of the bulk-W JET outer divertor target tiles was deliberately misaligned to height of $\sim$1 mm and exposed to a series of high power H-mode discharges. The experiment hoped to observe transient (ELM-driven) melting for the first

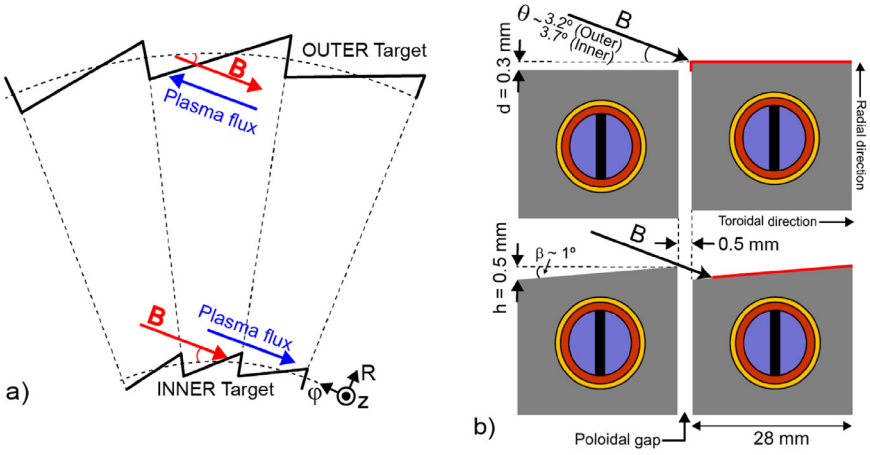

Fig. 2. Schematics illustrating the global target tilting (a) and (b) examples of misaligned unshaped (upper) and shaped (lower) toroidally neighbouring MBs giving typical field line angles and main geometrical parameters. The red bold lines on the MB surface indicate the zones of thermal plasma loading in each case.

time and to investigate the dynamics of melt motion and any evidence for melt splashing and droplet ejection It succeeded spectacularly in demonstrating dynamic melting on the ELM timescale and subsequent modelling with the MEMOS-3D melt code reproduced rather well the observed melt motion and final lamella erosion profile, giving confidence that this code, which is used extensively for ITER calculations (see Sections 3.3 and 3.4), can be trusted.

However, discrepancies were apparent early on in the JET experiment between the parallel heat flux required to reproduce the misaligned lamella surface temperature (only the top surface of the lamella was visible with an infra-red (IR) camera observing the lower divertor from the top of the vacuum vessel) and that derived from observations on non-misaligned surfaces. So called "mitigation factors", or perhaps more correctly, "reduction factors" (0.2 for L-mode and 0.4 for H-mode [14]) were derived from these measurements by using MEMOS-3D to generate temperature profiles based on the input heat fluxes and from them producing synthetic signals to compare with the IR data (accounting for issues of limited spatial resolution on the lamella top surfaces).

At the time of the analysis and reporting of the experiments, the factors were not understood. A detailed PIC study, for example, found that ELM ion Larmor orbit effects were by far insufficient to explain the discrepancy in H-mode [15], and no such effects could even be invoked for L-mode, where local plasma temperatures are low, and ion Larmor orbit radii small in comparison with the misalignment. This then cast doubt on the understanding of plasma interactions on LEs at low magnetic field incidence angle and hence on the applicability of the physics approach to ITER divertor MB shape assessments. As a result, a multi-machine coordinated task was launched in 2014 through the International Tokamak Physics Activity (ITPA) Divertor and Scrape-off Layer (SOL) Topical Group to investigate the edge power loading issue. The first part of this paper summarizes the findings available at the time of writing from this multi-device collaboration, including some discussion of a new look at the primary JET experiment which has revealed some issues with the original thermal analysis.

The second part of the paper returns to the question of shaping in the ITER context, assessing in more detail the pros and cons of shaping with particular emphasis on the issue of melt damage, both transient and steady state, with and without shaping. The application of even a simple toroidal bevel as in the current baseline vertical target design is an additional complexity in the manufacturing exercise and must be properly justified from the physics/operational standpoint.

2. Multi-machine leading edge experiments

In support of the physics basis for the ITER MB shaping decision and stimulated by the JET deliberate misalignment experiment [14], a dedicated coordinated task was established at the beginning of 2014 within the Divertor and SOL ITPA Topical Group. Several tokamaks (JET, ASDEX-Upgrade, KSTAR, DIII-D, COMPASS) together with the linear devices Magnum-PSI and Pilot-PSI responded to this call, in all cases requiring the provision of dedicated hardware and experimental time. The primary aim was to investigate the LE power loading at glancing angle studied first at JET, with emphasis on maximizing IR diagnostic capability to best resolve the surface temperature in the vicinity of the edge which was limited in the JET experiment due to the long distances between the divertor and the IR camera. Tokamak studies were to be performed, where possible, in both L-mode and H-mode and magnetic field line incidence angles in the range relevant to the ITER burning plasma equilibrium ($\alpha = 3.2°–3.7°$ - Fig. 2b) accounting for global target tilting). A second goal of some of the experiments was to study the dynamics of transient-induced melting. This aspect will be discussed in Section 3.2.

A common feature of all these experiments is the restriction that the key experimental information (surface temperature) measurements, is obtained in almost all cases using IR cameras viewing the LE from above. The loaded edge itself cannot therefore be observed and thermal analysis is required to match the measured T_{surf} on the top surface with an inferred $q_{||}$ impinging on the misaligned edge (arriving at near normal incidence) and on the surface (deposited at glancing incidence). The input $q_{||}$ is usually obtained from IR measurements elsewhere on a non-misaligned surface far away from any of the perturbing effects of the LE. The parallel heat flux is then obtained geometrically from $q_{||} = q_{\perp}/\sin\alpha$, where α is the impact angle between the total magnetic field and the surface, taking into account any geometrical factors of the surface being observed. For sufficiently high IR spatial resolution, such analysis can usually be performed without the corrections which were necessary in the JET case (convolution with the IR camera modulation transfer function [14]).

In a relatively short paper, it is not possible to describe the details and results from all the various ITPA experiments. Moreover, in some cases analysis of results is still underway at the time of writing and the conclusions insufficiently mature to be included here. Some of the experiments are described in accompanying papers [16-17]. A brief summary of key results from the LE experiments on the COMPASS tokamak [17] and on the

linear device Magnum-PSI are described below as representative of these ITPA studies, together with a word on the current status of the experiments at JET. Preliminary analysis of results from KSTAR for inter-ELM power loading [16] support those found on COMPASS and Magnum-PSI. An initial experiment on DIII-D using the DiMES divertor manipulator to insert three W blocks carrying two different misalignments (d = 0.3 and 1.0 mm) was hampered by an IR camera defocusing problem, but also concluded that in L-mode, LE power loading could be described geometrically [18]. A second, much improved experiment in Type I ELMing H-mode, including time resolved ELM measurements, has been performed and is currently being analysed. Further experiments building on the first experience at KSTAR are also underway, with the primary aim to study ELM resolved power loading and to investigate a wider range of castellation geometries, including toroidal bevels as planned for the ITER monoblocks. Finally, an extensive study [19] has been performed on ASDEX Upgrade, in which special W lamellas, almost identical in design to those of JET, were exposed in the outer divertor target to ELMing H-modes.

2.1. COMPASS

The COMPASS team have concentrated efforts on the observation of misaligned edge loading in limiter plasma equilibria, using a series of specially manufactured inner wall graphite limiter tiles directly in the field of view of a high resolution IR system (0.3 mm/pixel) mounted on an outboard midplane port [17]. The latest in these series of special limiters is a symmetric roof top design (see Fig. 1 of [17]), mounted symmetrically at the inboard midplane, and protruding 6 mm radially inwards compared to the toroidally neighbouring tiles. The rooftop slope angle is fixed at 2.5°, but a 1° tilt due to mounting tolerances on the central column, gives an inclination of 1.5° on one side of the tile and 3.5° on the other.

Machined into each of the 4 quadrants (above and below the inboard midplane and on each rooftop) are a set of four poloidal gaps with deliberate misalignments d = 0, 0.3, 0.6 and 1.0 mm. The gap with d = 0.6 mm is also arranged such that a small "pocket", or depression, is machined into the tile body just to the downstream side of the gap. This is intended to simulate the original misaligned lamella experiment at JET [14], in which several of the lamellas in front of the misaligned edge were depressed in order to allow field line penetration to the edge. This pocket in front of the misalignment was qualitatively advanced as one of the possible explanations for the observed parallel power flux discrepancies (Section 1) observed in the JET experiment, with the reasoning being that the depressed surface might lead to enhanced cross-field transport into the "mini-SOL" caused by the pocket and hence reduce the parallel heat flux to the exposed lamella.

The key result of this latest COMPASS experiment [17] is neatly summarized in Fig. 3, which gives the measured IR temperature profile along a toroidal line across the 3.5° inclined rooftop in the tile quadrant containing the poloidal gap with 0.6 mm leading edge and the machined depression. The "synthetic" signal also plotted in Fig. 3, is a rather sophisticated reconstruction using 2D finite element (FE) calculations (using the code CASTEM) to match the measured T_{surf} on an unperturbed region of the tile far downstream of the gap and convoluting the numerical profiles with a modulation transfer function specific to the IR camera, taking into account radiative perpendicular loading. A key assumption in this process is that power deposition is geometrically optical everywhere, including on the LE. That is, ion Larmor radius effects (ρ_L ~0.8 mm for these COMPASS conditions (toroidal magnetic field, $B_\varphi = 0.9$ T) and thus comparable to d and the gap width) are neglected. Fig. 3 evidently shows that the synthetic signal is a close match everywhere to the measured power flux density (recalling that the IR camera

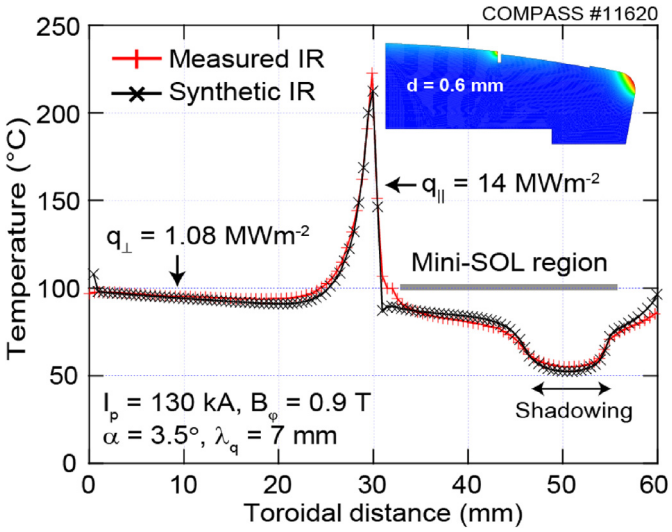

Fig. 3. Composite showing the key result from the COMPASS leading edge studies on a specially designed graphite inner wall limiter tile [17] in which geometrical power loading is closely followed and no discrepancies are found in a depressed ("mini-SOL") region preceding a LE with d = 0.6 mm.

does not directly observe the misaligned edge), including the machined pocket in front of the LE. The observations of power deficits seen at JET are thus not reproduced, the optical approximation (OA) is valid and the presence of a local depression ("mini-SOL") does not appear to affect the impinging parallel power flux.

The COMPASS team have supported these high precision IR measurements and power flux deconvolution with PIC simulations using the in-house SPICE code, taking as input values of local plasma temperature and density measured in previous similar discharges using an instrumented limiter tile [17]. These code simulations demonstrate that ion Larmor radius smoothing should be occurring in the immediate vicinity of the leading edge under the COMPASS experimental conditions (this is expected for $d/2\rho_L < 1$ [20]), but the discrepancy between the PIC computed T_{surf} and the IR measurements, themselves matched almost perfectly by heat transfer calculations based on the OA, indicates that the PIC assumption of heat conduction dominated by ions ($q_{tot} = f^*q_i + (1-f)^*q_e$, with f = 5/7 [17]), and hence of ambipolar conditions, is not justified. A dominant electron contribution (and therefore non-ambipolar conditions), which would match an OA assumption due to the small electron Larmor radius, is one possible explanation. This is being further investigated.

2.2. Magnum-PSI

Leading edge loading has been studied in a series of dedicated experiments on the Magnum-PSI linear device in which an inclined, water-cooled, castellated target bearing a series of W blocks misaligned by d = 0.0, 0.3, 0.6 and 1.2 mm has been exposed to plasma at impact angles in the range $\alpha = 4°–8°$ and observed by a near-perpendicularly viewing IR camera with 0.4 mm/pixel resolution [21]. Plasma parameters are those characteristic of expected values in the strike point vicinity of semi-detached ITER burning plasmas ($T_e = 3$ eV, $n_e = 1.3 \times 10^{20}$ m^{-3}) at a magnetic field of 0.35 T (thus $\rho_L \sim 0.5$ mm), giving values of the ratio $d/2\rho_L = 0–1.2$, covering the range over which Larmor smoothing of edge power loading should occur.

An example of the experimental results, for $\alpha = 5°$ is compiled in Fig. 4, showing that for all misaligned cases, the IR heat flux profiles along the misaligned block top surfaces are well matched by calculated curves obtained from ANSYS FE analysis (fully ac-

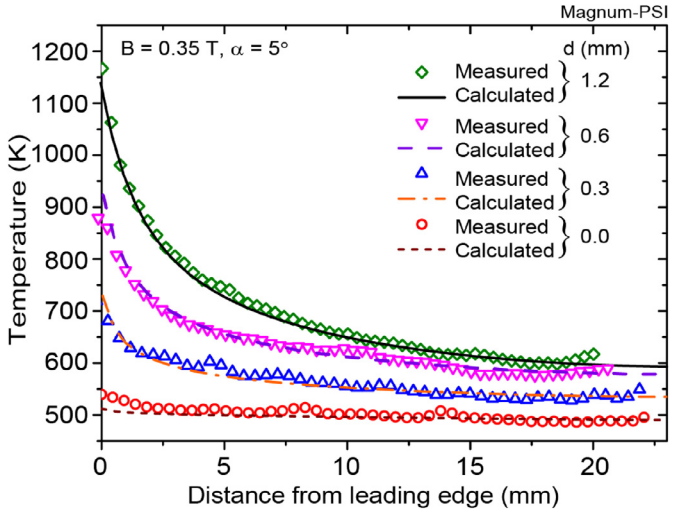

Fig. 4. Comparison of measured and computed surface temperatures on W blocks misaligned to varying degrees (d = 0 → 1.2 mm) in the Magnum-PSI linear device. Geometrical power loading is satisfied to within 1.5% [21].

counting for the water-cooled environment). This is performed by first using the FE code to derive the incident $q_{||}$ from IR T_{surf} measurements on a flat plate (solving the inverse heat conduction problem), then using the OA together with ANSYS to impose this $q_{||}$ onto the misaligned blocks and comparing with the experimentally measured T_{surf}. The OA is computed to be satisfied to within 1.5% from the data in Fig. 4. Although PIC simulations are not available for these Magnum experiments, calculations have been performed in which the Larmor smoothing effect is simulated by an increase in heat load on the top surface near the misaligned edge on the scale of ρ_L, balanced by a decrease on the LE to preserve power balance. The result is that such local heat load modifications cannot in any case be resolved by the IR system.

2.3. JET

As mentioned in Section 1, it was discrepancies in the derived power loading to the JET misaligned lamella experiment [14] which stimulated the multi-device ITPA coordinated task. In an effort to resolve the issue and to gain more insight into ELM-induced surface melting, a second special lamella experiment was proposed at JET and installed in 2015.

Fig. 5a and b compare the old and new geometries, in the form of thermal maps derived from FE simulations obtained using the Abaqus 3D software [22]. Detailed thermal analysis [23], exploiting the new, simpler lamella geometry, benefiting from improvements to the IR viewing hardware (notably improvements in system focus and resolution), properly accounting for several geometrical factors (magnetic field and proper description of the lamella 3D structure) and the introduction of an as yet unexplained "isotropic" fraction of the SOL $q_{||}$ seen with the improved IR in the magnetic shadow behind the special lamella (a more important contribution in H-mode), finds no $q_{||}$ discrepancy in either L-mode or H-mode (including during ELMs).

A separate, complementary but quite different approach using ANSYS FE analysis exploiting the same experiments on the new lamella geometry, but so far for L-mode only, similarly finds no discrepancy [24]. Both methods conclude that the OA is satisfied to within ~10%. Fig. 5c gives an example for the L-mode generated using the analysis procedure described in [23], comparing the temporal evolution of the measured IR and calculated surface temperatures at the peak of the heat flux pattern on the top surface of the old lamella during pulse JPN 84514.These new analysis tools devel-

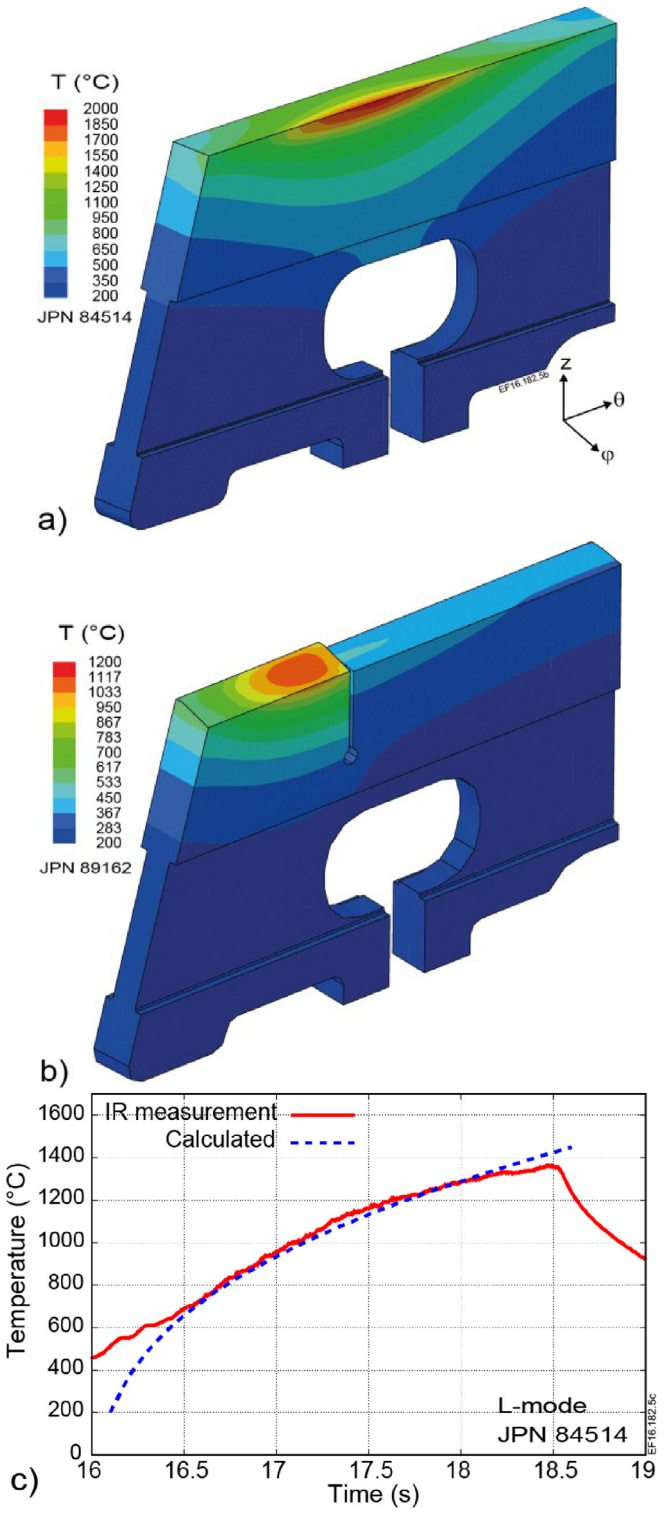

Fig. 5. FE temperature maps of the special W lamellas in the JET bulk W outer divertor computed with the Abaqus code using experimental $q_{||}$ input profiles: (a) the original misaligned component with d ~1.0 mm and (b) the most recent design with a 15° slope. More sophisticated analysis techniques and improved diagnostics put in place for the latest experiment and applied retrospectively to the 2013 study have eliminated the apparent discrepancies in the input $q_{||}$ such that geometric loading is now consistent with the measurements [23,24]. This is shown in (c) which compares for an L-mode pulse in the original experiment, the temporal variation of the peak temperature on a poloidal line in the centre of the misaligned lamella in (a) compared with the expected value from the FE calculation.

oped to model the second lamella experiment, together with the experience gained from the latest measurements, seem to show, in fact, that the parallel power fluxes in the original experiment with the LE special lamella really are only a fraction of what they were thought to be using the IR data and analysis capability available at that time [23]. Nevertheless, the "reduction factors" on $q_{||}$ reported in [14] required to bring the MEMOS-3D computed surface temperatures in line with IR measurements appear to be understood. An OA for the original JET misaligned lamella experiment is thus now also consistent with the measured data.

3. Importance of monoblock shaping

As the previous section has shown, all experiments to-date conducted under the ITPA multi-machine study have concluded that geometrical power loading on poloidal gap LEs can be assumed, at least within measurement capabilities for stationary loading cases (e.g. L-mode or inter-ELM H-mode). Of the ITPA experiments which have explicitly addressed the ELM transient loading question, ASDEX-Upgrade reports that the OA also holds in this case [19], as does the new treatment of JET data from the previous misaligned lamella experiment (Section 2.3). Analysis from DIII-D and KSTAR is still underway at the time of writing.

Under the assumption of geometric power loading, and excluding the issue of toroidal gap loading during ELMs (dealt with in detail in [10,11]), an assessment can now be made of the importance of shaping the ITER MBs to protect inter-PFU radial steps at poloidal gaps (Section 1 and Fig. 2b). The arguments are best made by separate discussions which consider loading either of an exposed poloidal gap (in the case in which no shaping is applied) or for a surface bevelled in the toroidal direction, without taking into account melting or melt dynamics (Section 3.1) and then asking what would be the consequences of melting in both cases (Section 3.2).

3.1. Stationary loading in the absence of melting

Fig. 6 compiles a series of four 3D ANSYS FE simulations of standard ITER tungsten MBs, assumed here to have a minimum of 6 mm W thickness from the top surface to the Cu interlayer between the W and the CuCrZr cooling tube. This thickness is a compromise between keeping the steady state T_{surf} as low as possible for given incident heat flux and maintaining acceptable margins against the achievement of critical heat flux at the cooling interface in the event of slow transients and avoiding the overheating of Cu during heavy fast transients (disruption induced heat fluxes). The four cases comprise unshaped (Fig. 6a and b) and shaped (Fig. 6c and d simple toroidal bevel of Fig. 2b) MBs for two values of $q_{\perp}$ on the top surface (the incident heat flux impinges from the left hand side in all cases). For the purposes of this comparison, the MBs are assumed to be at the outer target, where inter-ELM heat fluxes are expected to be highest, even if the total angle of impact is lower than at the inner (3.2° at the strike point including global target tilting). The blocks are assumed to be uniformly heated in the poloidal direction with no contribution from power deposition on toroidal gap edges which is predicted when ion Larmor orbits are properly accounted for [10,11]. In all cases, the MBs are assumed to be misaligned by the maximum nominal radial displacement of 0.3 mm.

As shown by the inserts in Fig. 6a–d, the input top surface heat fluxes are adjusted such that $q_{||}$ remains constant for each pair of cases, fixed to the value corresponding to $q_{\perp} = 10\,MW\,m^{-2}$ (nominal peak steady state power handling limit) and $20\,MW\,m^{-2}$ (nominal slow transient) in the axisymmetric case (i.e. without MB shaping or target tilting). This is because the plasma boundary simulations which have been used to define the maximum expected peak stationary target heat flux densities for burning plasma operation [3,4], do not include target shaping.

For the bevelled MB, a magnetically shadowed region exists over which thermal plasma impact is absent, but on which photonic radiation and charge-exchange fluxes will impinge in the real situation of a dissipative divertor. The sharing between thermal plasma and photonic/CX loading is sensitively dependent on the level of detachment and on the way in which it is achieved. For example, SOLPS code simulations for the ITER burning plasma with 100 MW of SOL power using neon (Ne) seeding for radiative dissipation to give a peak $q_{\perp} = 10\,MW\,m^{-2}$ at the outer target find very low radiative/CX target heat loads, with the majority of the power deposited by thermal plasma. In contrast, simulations using nitrogen (N_2) seeding for the same input power and peak $q_{\perp}$ show that, at the strike point, 40% of the heat flux density is due to photons and CX neutrals. This closely resembles the behaviour seen in the simulations when carbon is used at the divertor, as expected given the similarity of radiation functions between carbon and nitrogen.

In the sense that the strike point heat flux is more equally shared between the thermal plasma component (which follows field lines) and the more uniform perpendicular CX/photonic component, N_2 is a favoured option for seeding. Experimentally, on current all-metal tokamaks, N_2 is also observed to permit recovery of the confinement loss seen when switching from carbon to metal plasma-facing components [25]. This is not in general yet the case for Ne, most likely as a direct or indirect consequence of increased power loss outside the divertor in comparison with N_2. Although this complicates life on ITER due both to the need to handle tritiated ammonia and the impact on duty cycle as a result of accumulation of ammonia in the divertor cryopumps (requiring regeneration to higher temperatures to release the ammonia), there is no obstacle to the use of N_2 in terms of the plant. It is, however, worth pointing out that integrated modelling using SOLPS to set boundary conditions for a core transport model does not exclude the use of Ne on ITER with regard to achieving the required plasma performance [26]. The ITER divertor is large compared with current devices and although Ne does not radiate as close to the targets as N_2, the impurity is well confined confined according to the simulations. More refined studies need to account for the influence of fluid drifts, which may strongly influence the impurity transport. Such work has started for ITER using the SOLPS-ITER code with drifts activated [27].

For illustrative purposes, the N_2 simulation case is used here so that for the unshaped, misaligned MB (Fig. 6a) and a nominal stationary $q_{\perp} = 10\,MW\,m^{-2}$, $q_{||} = 6/\sin(2.7) \sim 127\,MW\,m^{-2}$ (only 60% of the top surface heat flux carried by thermal plasma, $\alpha = 2.7°$ without target tilting or shaping), and when the 0.5° global outer target tilt is added, $q_{\perp} = 4 + 127\sin(3.2) \sim 11\,MW\,m^{-2}$. In the slow transient, attached divertor case (Fig. 6b), the radiative/CX component is absent and the nominal $q_{\perp} = 20\,MW\,m^{-2}$ requirement yields $q_{||} = 20/\sin(2.7) \sim 425\,MW\,m^{-2}$ which is incident essentially perpendicularly on the misaligned edge and leads to a top surface loading of $q_{\perp} = 425\sin(3.2) \sim 24\,MW\,m^{-2}$ due to the global tilt.

The same reasoning is applied to the bevelled MB, but now, due to the shaping, 8% of the top surface is shadowed, receiving, for the nominal stationary $q_{\perp} = 10\,MW\,m^{-2}$ case (Fig. 6c), only $4\,MW\,m^{-2}$ of photonic/CX loading. The remaining, non-shadowed portion receives $q_{\perp} = 4 + 127\sin(4.2) \sim 13\,MW\,m^{-2}$ with the total angle now increasing by 1° due to the toroidal bevel. In the slow transient case with shaping (Fig. 6d), radiative/CX loads are absent, there is no power in the shadowed region and the remainder of the surface receives the full thermal plasma component: $q_{\perp} = 425\sin(4.2) \sim 31\,MW\,m^{-2}$.

All simulations have been performed taking into account the full temperature dependence of the W thermal properties (as-

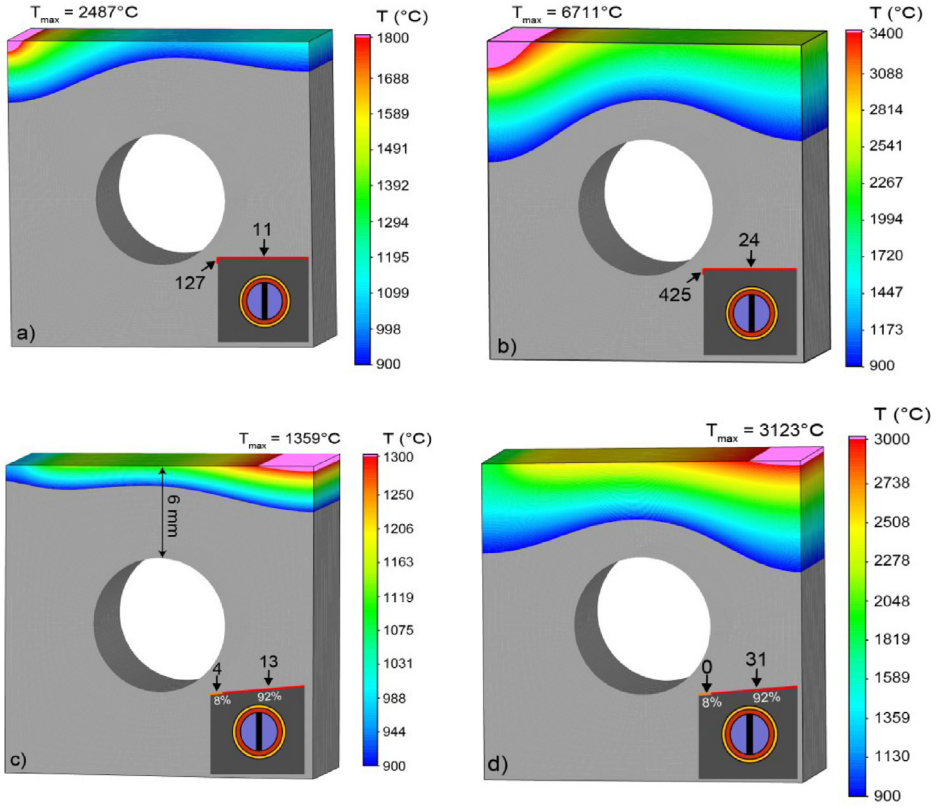

Fig. 6. ANSYS FE simulations of the temperature field in unshaped (a,b) and shaped (c,d) ITER water-cooled, outer vertical target tungsten MBs subject to nominal (a,c) and slow transient (b,d) heat fluxes. The insets in each figure illustrate the heat flux densities (MW m^{-2}) applied to the various parts of the surface (see main text). Note that the magenta zones include all temperatures higher than the maximum values in each colour bar – the maximum temperature achieved in each simulation is indicated. The input heat flux impinges from the left and the worst case radial misalignment of 0.3 mm is assumed in all cases. (For interpretation of the references to colour in this figure legend, the reader is referred to the web version of this article.)

suming stress-relieved W material) and the nominal ITER divertor cooling parameters. In all cases, the loading duration is 10 s, by which point a steady state temperature field has been readily achieved (typically after 5–6 s for both values of $q_\perp$). The full simulation methodology may be found in a more detailed account [28].

The results illustrate the trade-offs between shaped and unshaped surfaces under stationary power flux densities. An important criterion for comparison is in terms of the recrystallization temperature T_{recrys}. Recrystallization is a thermally activated process in which the material crystal structure is modified due to the nucleation and growth of new, strain-free grains (grain growth), reducing the internal residual stress of the material. The process is associated with a reduction in material strength/hardness, shock resistance and an increase in ductility [29] and is a function of time at any given temperature [30]. For any given material, T_{recrys} is a strong function of the deformation history and can vary over a large range (e.g. from $T_{recrys} \sim 1000\,°C$ – 1700 °C for ITER grade W depending on how it is produced [31]). An important consequence of operation at temperatures beyond T_{recrys} is the development of MB macro-cracking, which has now been linked to the loss of strength due to recrystallization [32].

The focused heating at the left hand corner of the unshaped, misaligned MB is clearly visible in Fig. 6a, with maximum temperatures at $q_\perp = 11\,MW\,m^{-2}$ of ~2500 °C, still far below melting for W ($T_{melt,W} \sim 3422\,°C$). At the higher "slow transient" heat fluxes (Fig. 6b) a large zone around the misaligned corner is far above $T_{melt,W}$and a significant region of the block surface, down to a depth of several mm, reaches temperatures well above the maximum of T_{recrys}. In reality, such extreme melt depths will not occur given the very strong melt motion which is expected to develop at the corner and which would almost certainly severely impact the plasma. In fact, melt temperatures are attained very quickly in these simulations, after only ~0.1 s (even for a starting condition at $T_{surf} = 70\,°C$, the standard cooling water inlet temperature). Section 3.4 will look more closely at the consequences in terms of melt motion under stationary loads.

Returning to the misaligned case at nominal $q_\perp$, an important observation is the presence of a significant volume of material in the LE vicinity at temperatures in the range of or above T_{recrys}. Since the misalignment is a permanent feature once the unshaped block is installed, even if edge melting is easily avoided (due to the water cooling), prolonged, high power operation will unavoidably result in recrystallization over a sizeable region (recrystallization is a function of both temperature and time). For the shaped MBs, the LE is of course protected, at the price of higher stationary temperatures at the right hand corner due to the bevelling (Fig. 6c and d). At nominal $q_\perp$ (Fig. 6c), however, T_{surf} ~1300 °C, which is approximately at or below the value of T_{recrys} found in tests of a series of W products each satisfying the ITER material specification [30]. At higher $q_\perp$ (Fig. 6d), although a large volume of the MB reaches temperatures $\gg T_{recrys}$, melting of the top surface is marginally avoided.

Although the preceding arguments serve to highlight the general pros and cons associated with shaping in the case of stationary, or quasi-stationary loads, the chosen example is only one of a whole range of possible front surface loading conditions. For example, as mentioned above, using Ne seeding in place of N in SOLPS simulations strongly modifies the relative contributions of radiative and thermal plasma loading in the divertor strike point region. This particular case of Ne seeding with peak $q_\perp = 10\,MW\,m^{-2}$ is

used in [10] for illustrative purposes, but now deploying the full 3D ion orbit model to describe the surface loading on shaped MBs, as opposed to the OA used here. Similar thermal calculations to those in Fig. 6c show that $T_{surf} > 1300$ °C across almost the entire surface, with a significant region in excess of 1500 °C. This is due to the increased thermal plasma flux density in the non-shadowed region and to toroidal gap edge heating which is manifest only if ion orbits are properly accounted for. The reality is that if shaping is used to hide misaligned poloidal gap edges, and if the criterion that the stationary MB temperature remain below T_{recrys} is to be satisfied, the increase in surface power flux density resulting from higher field line impact angles will have to be offset by a decrease in $q_{||}$. This can only be achieved through careful choice and control of the divertor plasma state and is likely ultimately to be manifest in operating instructions for the ITER machine.

3.2. ELM driven transient melting: experiment and interpretation

Assessing the impact of melting on ITER MBs can only be performed through numerical simulations. Thus far, all calculations performed in collaboration with the ITER Organization (IO) have employed the MEMOS (Melt Motion at Surfaces) melt code (see e.g. [33], in both its 2D and 3D versions. Experimental validation of the code in a tokamak was first achieved in TEXTOR for the case of steady state melting [34,35] and, as first discussed in Section 1, it has been very successful in reproducing the melt motion in the JET misaligned lamella experiment (see [14] and Fig. 7). This latter benchmarking is of particular importance for ITER in the sense that it was the first time a tokamak experiment had attempted to address the question of transient (ELM) driven melting, which, aside from disruptions, are the most likely conditions under which melting is expected to occur on the ITER divertor components [2].

The results of MEMOS-3D modelling for the JET experiment were first published in [14], in the form of a 2D distribution of erosion/melt accumulation, computed for a single discharge in the series of 6, near identical Type I ELMing H-modes to which the misaligned lamella was exposed. To compare with high resolution photographs of the final melt distribution, it was simply supposed that the computed melt motion for a single pulse could be multiplied by a factor 6 to account for the 6 identical discharges. The full calculation has now been done, taking into account the complete history of the measured time dependent heat flux, including all ELMs and the ramp-up and down phases on the lamella for the 6 consecutive discharges. The result is shown in Fig. 7a, which is the analog to Fig. 26 in [14], and should be compared with the photographed final erosion/melt profile included as an inset in the same figure. A heat reduction factor of 0.4 on the $q_{||}$ incident on the misaligned edge is applied here as in [14], ensuring a good match between the surface temperatures and W vapourization computed by MEMOS-3D and those measured experimentally. As discussed in Section 2.3, it now appears in the light of new analysis that this factor is essentially fully understood so that the values of $q_{||}$ used in these MEMOS-3D simulations are correct.

Even though the MEMOS-3D output can only match the approximate displacement and accumulation of material (and cannot hope to reproduce the fine structure seen in very high resolution photography of the melted lamella), it is extremely encouraging that the simulations should be able to reproduce the gross material damage profile. A key observation is that the accumulation of melted material occurs primarily along the perpendicular LE, showing that the large melted region normal to the magnetic field lines is the primary source.

What is most important in this code-experiment benchmarking exercise with regard to extrapolation to ITER is to have confidence in the mechanism predicted by the code to qualitatively explain the JET melt observations. The various forces at play on the melt

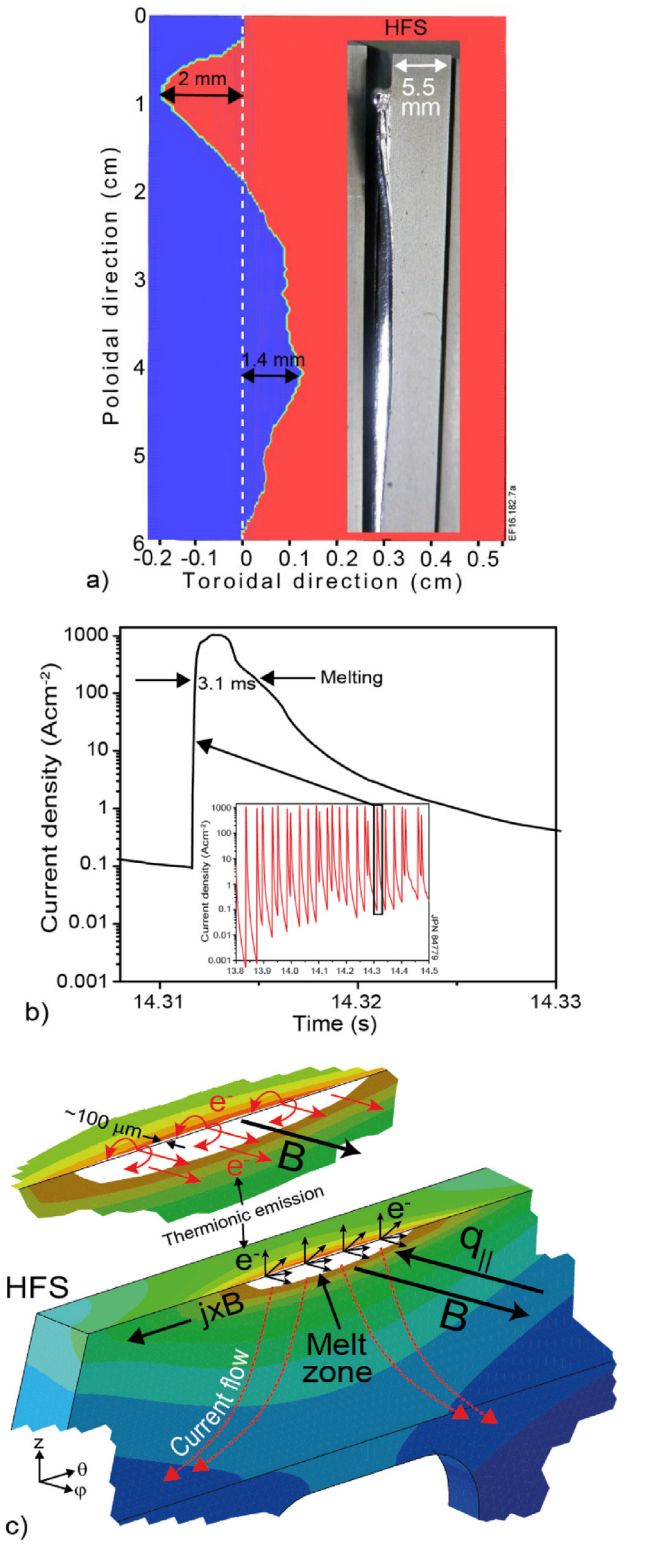

Fig. 7. Melt erosion and dynamics in the JET misaligned W lamella experiment. (a) MEMOS-3D simulations of final erosion profile after 6 near identical Type I ELMing H-mode discharges with inset high resolution photo of the lamella recovered from the machine. (b) Calculated thermionic current density during a single ELM in one of the 6 pulses – the inset shows the time dependence across several tens of ELMs. (c) Schematic illustrating the electron emission from the melted zone on the lamella edge with zoomed region showing grossly exaggerated electron trajectories. Note that the electric current direction in the material is defined according to the standard convention.

layer and the input modelling assumptions were already clearly described in [14]. Two key factors permit agreement with the experimental melt displacement: the inclusion of vapour shielding driven by intense W evaporation during the ELM impact on the misaligned edge, and the $\mathbf{j}\times\mathbf{B}$ force on the melted layer, driving material towards the high field side (HFS) of the misaligned lamella. Here, j is mostly due to the thermionic current, emitted from the hot melted surface, whose temperature is computed to reach ~4000 °C or higher at the ELM peak (well above $T_{melt,W}$). Fig. 7b gives an example from the MEMOS-3D calculation of the mean thermionic emission current density along the leading edge during the ELMing phase of one of the JET discharges in the sequence reported in [14]. This current, j_e, is computed in accordance with the Richardson–Dushman law [36,37] at all points on the melted surface:

$$j_e = A_{RD} T_{surf}^2 \exp\left(-\frac{e\varphi_{work}}{kT_{surf}}\right) \quad (1)$$

with A_{RD} Dushman's constant, φ_{work} the work function (e.g. $\varphi_{work,W} \sim 4$–5 eV) and T_{surf} is in K. The current is predicted to reach ~10^3 Acm^{-2}, more than a factor 10 higher than that arriving at the surface during the ELM due to the plasma.

The $\mathbf{j}\times\mathbf{B}$ force generates melt motion towards the HFS along the poloidal direction with peak velocities up to 1.5 ms^{-1}, a factor of 250x the velocity due to the pressure of the impacting ELM plasma and the gradient of surface tension in the melt layer. Without this $\mathbf{j}\times\mathbf{B}$ drive, the total computed surface topology variation does not exceed ~20 μm after a full discharge with ~50 ELM events, orders of magnitude below the observed melt erosion and in the wrong spatial directions.

A detailed model of the emitted electron dynamics giving credibility to this MEMOS-3D calculation has not yet been provided and would be challenging, probably amenable only to numerical simulations (e.g. PIC). An attempt to describe the process schematically is presented in Fig. 7c, which uses the FE simulation model of the misaligned lamella in Fig. 6a to illustrate the basic idea, together with the approximate melt extent computed with MEMOS-3D. The intense ELM impact on the lamella LE produces a reasonably large melted zone, which extends only ~100 μm onto the top (flat) surface, far below what could be resolved by the vertically viewing IR camera whose pixel resolution is ~1.5 mm. Thermionic electrons are emitted everywhere from this melted region, in all directions at energies characteristic of the surface temperature (thus only ~0.4 eV). Those which are emitted from the largest melt region, which is almost perpendicular to the incoming plasma stream (and to **B**), will almost always be pulled away from surface by the local sheath electric field and are subject to little or no electromagnetic drift force. They therefore constitute a net current away from the surface and would force a "replacement" current to be driven throughout the melt region, providing the drive to push so much melted material laterally. The current must flow through the grounded lamella towards the surface as indicated approximately in Fig. 7c (which employs the usual convention for electric current direction), though this simple picture of the situation offers no explanation of return current paths, which must of course be present. Presumably in this JET experiment, a large fraction of the current might return to the toroidally adjacent (non-misaligned) lamella across the 1 mm gap between them, requiring some degree of anomalous cross-field diffusion. An experiment to confirm this hypothesis would be a major step in lending credibility to the explanation put forward here, as would the possibility to measure the current flowing through the lamella (see below).

As for the electrons emitted from the corner region and top surface of the melted lamella, they would find themselves moving at an angle to **B** and may return to the surface after less than one Larmor gyration, thus no longer contributing to the net emitted current. It should be clear that the schematic in Fig. 7c cannot be a faithful account of the true current pathways in the material of the lamella. In particular, the details of how the electron current turns towards the melt layer surface on the LE could only be derived by much more detailed calculations. What matters, however, for the melt motion drive proposed here is that some component of the current flow in the LE melt zone be in the direction perpendicular to the incident magnetic field. The MEMOS-3D calculations do not yet account for the distribution of current flow in the material and simply assume, for the purposes of computing the forces on the melt layer, that in the bulk of the melt region the a sufficient fraction of the replacement current is flowing vertically through the material.

In support of the assumption of thermionic electrons escaping the melted surface, one may use the well-known Child-Langmuir [38,39] law which sets the limit on the maximum electron current which can be emitted from a surface for given potential difference between the plasma and surface (in this case across the sheath): $j_{CL} = \frac{4}{9}\varepsilon_0\sqrt{\frac{2e}{m_e}}\frac{V_s^{3/2}}{\lambda_D^2}$ with $\lambda_D = (\frac{\varepsilon_0 T_e}{en_e})^{1/2}$ the Debye length (T_e in eV), here assumed as an approximation to the sheath width, and V_s the potential drop across the sheath. Assuming $V_s \sim T_e$, simplifying and evaluating constants yields $j_{CL} = 4.2\times10^{-14} n_e T_e^{1/2}$. Values for T_e and n_e during the ELM are not available for the JET melting experiment, but a recent study [40] in Type I ELMing discharges (at similar input power (~20 MW) though at lower plasma current, $I_p = 2$ MA cf. 3.0 MA in the melting experiment) using coherently averaged divertor target Langmuir probe signals found T_e ~25 eV and $j_{sat} \sim 7\times10^6$ Am^{-2}, implying a sheath edge density of $n_e \sim 9\times10^{20}$ m^{-3} and $\lambda_D \sim 1$ μm. This gives an approximate maximum current admitted across the sheath of $j_{CL} \sim 2\times10^4$ Acm^{-2}, much higher than the maximum thermionic emission current computed by MEMOS-3D at the ELM peak (Fig. 7b). This must be considered, however, as an extremely conservative estimate given that for current flowing in the sheath, the width would increase and the voltage would decrease. A space charge limitation on the Richardson emission current is thus not imposed in these MEMOS-3D simulations for JET. In fact, the model adopted in MEMOS-3D for space charge limitation follows the theory in [41]. Switching it on for the JET case has no effect on the magnitude of the emitted current. Without the current flow through the melt implied by the thermionic emission, the code cannot even remotely match the experimentally observed melt motion.

The JET experiment stimulated efforts within the ITPA multi-device LE study to reproduce the effect. Fig. 8 shows two results, from an experiment [19] on ASDEX Upgrade in which a replica of the JET misaligned lamella (in W) was exposed to several Type I ELMing H-mode discharges using the outer divertor target manipulator to insert the sample (Fig. 8a), and from a study ([42] and Fig. 8b) on the Pilot-PSI linear plasma device using a misaligned aluminium (Al) block with d = 0.3 mm (to allow for easier melting and to test an ITER-like misalignment). An important aspect of the ASDEX-Upgrade experiment is the inclusion of shunts to measure the current flowing through the exposed element. In the case of Pilot-PSI, tokamak-like ELM pulses are imposed at near glancing incidence on the LE by pulsing the cascaded arc plasma source whilst simultaneously exposing the edge to steady state plasma flux, adjusting parameters to ensure that melting occurs only during the pulses.

On ASDEX-Upgrade, as in JET, gross melt motion is observed in the direction consistent with a $\mathbf{j}\times\mathbf{B}$ force driven by a strong current flow through the melt layer. Moreover, the ELM $q_{||}$ was similar to the values used on JET and the measured thermionic current is of magnitude consistent with melting during the ELMs only [19]. The final observed melt profile on the misaligned lamella (Fig. 8a) is practically identical to that found on JET (inset of Fig. 7a). Note

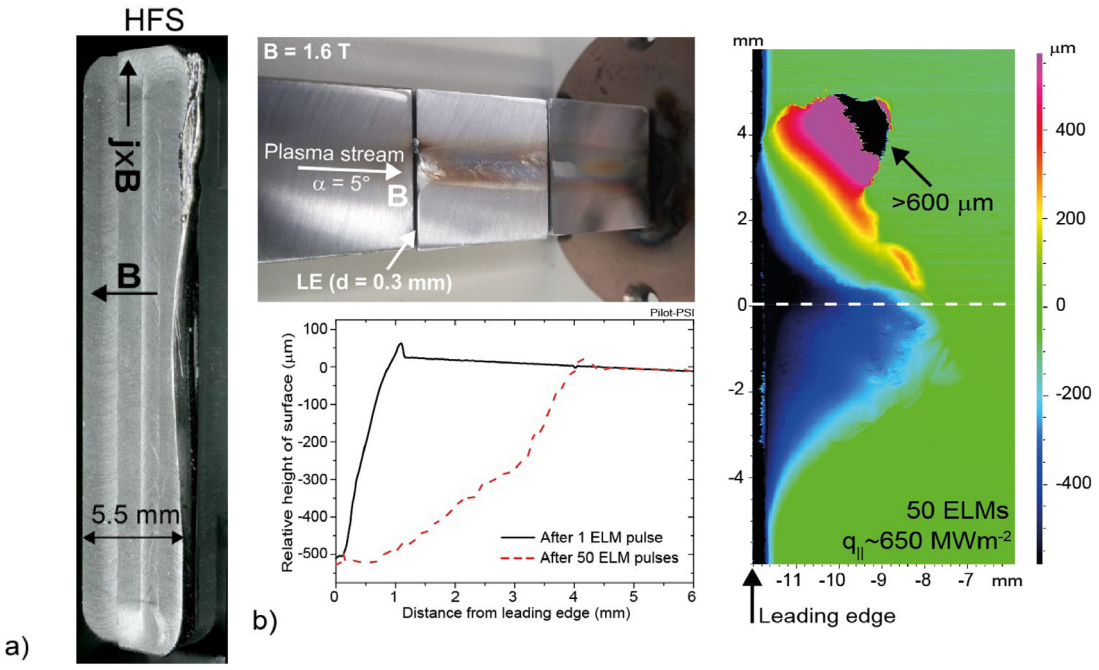

Fig. 8. (a) Photo of final melt erosion topology of the ASDEX-Upgrade misaligned sample. The resemblance to that from JET (Fig. 7a), of which the ASDEX-Upgrade experiment was a copy, is remarkable. (b) Melt studies on a 0.3 mm misaligned Al block in Pilot-PSI with (clockwise from top left): photo showing experimental configuration with post exposure melt damage, 2D profilometry across the misaligned block surface and 1D profiles taken from the leading edge across block surface showing clear deep erosion into the bulk after the 50 ELM-like pulses of the exposure.

also that the two experimental configurations (ASDEX-Upgrade and JET) differ crucially in the geometry: whilst in both cases B_φ is in the clockwise (or negative) direction, in JET I_p runs clockwise with the special lamella located in the horizontal outer target and is in the positive (anticlockwise) direction on ASDEX Upgrade with the LE installed in the outer vertical target. This means that to expose an edge in JET, the magnetic field vector must point away from the LE (Fig. 7c and [14]) and into it for ASDEX Upgrade (Fig. 8b). The (electron) current flow inside the lamella is thus vertically upwards in JET, leading to melt motion radially inwards, and radially inwards in ASDEX-Upgrade producing melt motion downwards. In both cases, this is in the direction of the private flux region and poloidally towards the HFS and is in each case consistent with some fraction of the replacement current compensating thermionic emission flowing through the melt layer with a component perpendicular to the top surface of the misaligned lamella.

In contrast, melt motion in the Pilot-PSI experiment (Fig. 8b) cannot be ascribed to thermionic emission. At melting temperature, the latter is many orders of magnitude weaker for Al compared with W, due to the inverse exponential dependence on T_{surf} in eqn. (1) ($T_{melt,Al}/T_{melt,W} \sim 0.2$ and the work functions for W and Al are similar). Moreover, given the geometry of the LE and magnetic field, the observed melt motion in Fig. 8b is in the opposite direction (it moves upwards, against gravity) to what would be expected if thermionic emission were the main driver as in the JET and ASDEX Upgrade experiments. This means that an alternative explanation is required for the melt motion. One plausible origin is the fact that because current cannot close in the Pilot-PSI cascaded arc source, it must return through the plasma, creating radial currents and electric fields which lead to strong radial gradients in plasma potential and deviations from ambipolarity across a conducting target surface (net electron current in the centre, net ion current near the periphery). This net inward directed electron current at the target centre would drive an upwards directed $\mathbf{j} \times \mathbf{B}$ force. Such currents have been measured [43] for targets perpendicular to the plasma beam, but never for the inclined targets used here. Melt layer motion driven by cross-field currents has been observed in separate experiments on Pilot-PSI [44]. It is possible that current flows could be further modified due to the break in symmetry introduced by a tilted target. Additional experiments are required to investigate this possibility and measure the currents, especially during the transient ELM-like pulses.

It might also be noted that the melt motion observed on beryllium (Be) limiters in JET during accidental melting events [45] could not be attributed to thermionic emission due to the low values of this emission for Be, similarly to the case for Al. The motion was instead suggested to be a consequence of the $\mathbf{j} \times \mathbf{B}$ force due to strong secondary electron emission (s.e.e.) from Be at the high plasma electron temperatures ($T_e \sim 40$ eV) characteristic of the neutral beam heated limiter plasmas in which the melting occurred. Two factors indicate that this same mechanism cannot be at work in the Pilot-PSI Al experiment: the observed melt motion is in the wrong direction and at $T_e \sim 15$ eV, the pulse plasma temperature is too low for s.e.e. to be significant.

Even if the melt motion in Pilot-PSI cannot be ascribed to the same thermionic emission processes as in the tokamak experiments, the results are key to the leading edge issue in showing how it is possible for erosion of an ITER-relevant exposed edge to progress at a rapid rate. The final erosion profile in Fig. 8b after exposure to 50 ELM-like pulses extends by several mm across the misaligned block in the plasma stream direction and to a depth exceeding the original 0.3 mm misalignment. This is direct experimental evidence that once edge melting begins, erosion may continue into the bulk of the material. This is also seen in the JET (Fig. 7a) and ASDEX-Upgrade (Fig. 8a) melt experiments, but in these cases the misalignment is rather extreme ($d \sim 1$ mm) so that an edge perpendicular to magnetic field lines is always guaranteed. Note that the Pilot-PSI experiment was conducted at $B = 1.6$ T in H plasma, giving $\rho_L \sim 0.35$ mm during the ELM pulses ($T_e \sim 15$ eV) and thus comparable to the misalignment height.

Modelling of the melt motion in the Pilot-PSI experiment is planned but has not yet been attempted and is complicated by the

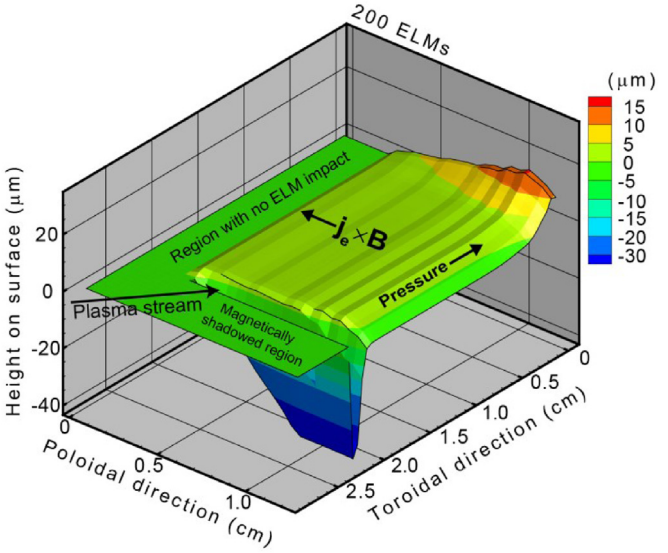

Fig. 9. MEMOS-3D simulation of final surface erosion profile for a single toroidally bevelled (h = 0.5 mm) ITER inner vertical target monoblock after 200 manufactured ELM transients with energy density 1.1 MJ m^{-2} just sufficient to provoke shallow, full surface melting. The ELM impact is randomly varied in the poloidal direction and the wetted area is irradiated uniformly (impact angle 4.7°). Geometrical loading assumed.

different (and not well known) current flows. One reason for the very severe propagation of the erosion region in the experiment may be that the transient heat flux densities drove the edge far above melting such that the natural "machining" of the edge caused by melt motion was insufficient to reduce the projected heat flux to values below which intense melting occurs given the low Al melting temperature (see Section 3.4).

3.3. Consequences of ELM driven melting on ITER monoblocks

As in Section 3.1 for stationary loads, the impact of ELMs should be considered from the point of view of shaped or unshaped MBs. For unshaped, misaligned blocks (assuming the standard 0.3 mm worst case LE), scoping calculations (not shown here) using 3D ion orbit modelling [10,11] taking input values of $q_{||}$ for mitigated ELMs during $Q_{DT} = 10$ operation from the current ITER heat load specifications [2], predict ELM heat loads on the exposed edge at least a factor of 5 above the W melting threshold. This is also true at half toroidal field ($B_T = 2.65$ T), when the first high power H-modes are expected on ITER in the non-active phases before nuclear operation begins [2]. Even for perfectly aligned MBs, ELM ions with large Larmor orbits are predicted to penetrate into gaps between them, depositing heat loads taking the edges above melting. If the ELM energy deposition in ITER were concentrated in a poloidal distance equivalent to just a single monoblock (width 1.2 cm), ~2000 MB poloidal gap edges would be exposed to potential melting at each ELM, with similar consequences regarding melt motion to those seen experimentally on today's devices (Section 3.2). Shaping using the 0.5 mm toroidal bevel in Fig. 2, alleviates the situation considerably, although ions on some orbits are still able to access the magnetically shadowed edge and the melt threshold during the transient can be marginally exceeded under some conditions [10]. From this point of view, it thus seems unwise not to shape the MB surface.

If shaping is employed, what then are the consequences if ELM driven melting does occur? By virtue of its successful validation against the JET lamella melt experiment, MEMOS-3D can be used to make an approximate assessment. As an initial study (Fig. 9), a situation has been manufactured in which ELM transients are imposed with energy density sufficient to melt the top, bevelled surface of a shaped MB. Geometrical power loading is assumed, so that ELM ion penetration into gaps (and possible subsequent edge melting) is absent and all locations on the impacted surface receive the same energy density. This is equivalent to assuming that the MB poloidal dimension is less than the ELM footprint and that there are no ion Larmor orbit effects which modify the power loading in the toroidal direction.

According to the existing ITER heat load specifications, helium H-modes at $B_T = 2.65$ T, $I_p = 7.5$ MA in the non-active phase of ITER operations are thought to be the first instances in which unmitigated Type I ELMs may provide high enough energy densities to produce full surface melting [2]. This may now have to be modified in the light of the new peak parallel ELM energy density experimental scaling for Type I ELMs [46], which is favourable for ITER and which suggests that there may be more margin against ELM-induced MB melting than previously thought. The conclusions below derived from MEMOS-3D modelling remain valid however, since at some point in the operational campaigns, uncontrolled ELMs will be sufficiently energetic to fully melt a divertor MB surface, even if this does eventually occur more at full toroidal field than for $B_T = 2.65$ T. A higher B-field will mean faster melt motion, due to $\mathbf{j} \times \mathbf{B}$ forces.

Helium ELMs at 2.65 T/7.5 MA are expected to have rise times on the target of ~350 μs, frequencies of ~5 Hz and plasma stored energy losses of ΔW_{ELM} ~4 MJ (the ELM fall time is chosen fixed at 350 μs) [2]. Time dependent modelling with the SOLPS-5.0 and JOREK codes indicates peak plasma pressures at the target during these events of ~4 kPa. Steady state (inter-ELM) power flux densities on the targets will be considerably lower in these plasmas than for $Q_{DT} = 10$ operation, so a stationary $T_{surf} = 700$ °C is assumed in the strike point region where the ELM peak power deposition occurs [2]. Since field line impact angles are steepest at the ITER inboard target (see Fig. 2), a total angle (including global target tilting and MB shaping) of 4.7° is taken as a worst case (B_T ~4 T at the inner target strike point location for half toroidal field operation). New measurements are also finding that the peak ELM $q_{||}$ at the inboard target might be slightly higher than at the outer [46].

A single, toroidally bevelled ITER divertor MB is modelled with MEMOS-3D, using the above input specifications and progressively increasing the transient energy density until shallow, flash melting just begins to occur on the MB top surface. This requires $E_{\perp,ELM}$ ~1.1 MJ m^{-2} on the surface, producing a melt thickness of ~17 μm existing for 500 μs. To produce a more realistic simulation of the likely surface damage after several such ELMs, the poloidal position of the ELM impact on the top surface is varied randomly between 0.3 and 1.1 cm. The final surface topology after 200 such events is shown in Fig. 9, where MEMOS-3D uses the damage profile after each event as input to the next.

These simulations differ from the JET modelling in that W vapour shielding is now absent due to relatively low evaporation rates (total computed evaporation after 200 events amounts to <0.08 μm). This is much lower than for the JET misaligned edge experiment. In common with the JET case, no space charge limitation is imposed, but because the melting now occurs only on the top surface, at glancing angles to the B-field, a significant fraction of the emitted electrons are expected to return back into the surface as a result of their gyromotion. In MEMOS-3D, a model describing the attenuation of net electron emission due to gyro-rotation at glancing angles [47] can be applied to describe this "compensation" effect on the thermionic emission current. It has been switched on to produce the simulation in Fig. 9 and reduces the thermionic current by about a factor 5. This in turn reduces the current flow through the melt layer which decreases the strength of the $\mathbf{j} \times \mathbf{B}$ drive. The combination of this effect with

the random poloidal impact location and the frictional force on the melt layer surface due to the plasma pressure pulse (flowing parallel to **B**), generates a final surface profile with similar topological modification in both toroidal and poloidal directions, compared with the very asymmetric result found in the presence of a LE. A total predicted surface elevation of ~15 μm after 200 melt events for the ITER MB is negligible in comparison with the erosion of the JET misaligned lamella on the mm scale after ~300 ELMs (Fig. 7a). Computed melt motion speeds are well below the estimated threshold for droplet splashing.

These results are of course valid for both shaped and unshaped MBs, if it is admitted that ELM energy densities sufficient to drive full surface melting may occur at some point during operations. The difference being that melting on unprotected poloidal LEs will be of much greater severity and will occur at much lower ELM energies. Note that 3D ion orbit studies indicate that melting of thin (few 100 μm) edge regions can occur on toroidal gap edges during ELMs, even at rather low ELM energy density at the targets [10]. A possible mitigation strategy in this case is the use of a "planar double bevel" in which the MB surface is shaped toroidally and poloidally. Studies of this option are still at an early stage at the time of writing, but show that the combined bevel option does have potential to mitigate the ELM toroidal gap loading problem at the outer target. At the inner target, however, this option is unlikely to succeed fully since the field and target geometry are such that ions and electrons flow to opposite sides of the toroidal gap and so both cannot be simultaneously shadowed. In all cases, the addition of a poloidal bevel further increases the magnetic field impact angle and hence the steady state and ELM-induced heat flux density everywhere on the unshadowed MB top surface.

3.4. Consequences of stationary melting on misaligned edges

Section 3.1 has considered the case of stationary loading on shaped and unshaped MBs, assuming baseline misalignments and imposing standard and "slow transient" heat fluxes. The emphasis there was on the consequences mostly in terms of the bulk temperatures likely to be attained in the MB and their proximity to T_{recrys}. Note that since the high values of $q_{\perp}$ imposed in these calculations can only be readily achieved in high performance plasmas, they necessarily apply only to the burning plasma phases of operation.

A deep melted region in the vicinity of the LE is evident in the FE simulation in Fig. 6b for an incident $q_{||} = 425\ MW\,m^{-2}$ (corresponding to an attached/high recycling divertor plasma). This is not a realistic simulation in the sense that the melted material would not remain intact for the long timescales of these FE simulations (in which $T_{melt,W}$ is already exceeded after ~0.1 s). To study the likely melt motion in the case of misaligned and unshaped MBs, recourse is again made to MEMOS-3D simulation, employing the same MB geometry and field line angles as in Section 3.3 for the ELM driven melting calculation, but now without toroidal bevelling and with a finer numerical mesh to properly resolve the very narrow region (300 μm) of the LE. As for the ELMs, this corresponds to the inner target, focusing on a slow transient (plasma reattachment) event in which the input heat flux density rises far above the value yielding the peak steady state $q_{\perp} = 10\ MW\,m^{-2}$. Since this is now appropriate to high performance plasmas, operation at nominal toroidal field and current is assumed ($B_T = 5.3$ T, $I_p = 15$ MA), giving B_T ~7.9 T at the inner target strike point. Plasma pressure is assumed to be zero in these stationary loading cases.

The procedure is similar to the ELM melting calculations: assume the OA and find a value of $q_{||}$ at which melting begins for given heating duration, but this time considering a 0.3 mm misaligned edge on an unshaped MB. A starting $T_{surf} = 1000$ °C is assumed, corresponding approximately to steady state operation at $q_{\perp} = 10\ MW\,m^{-2}$. The full MB cooling tube geometry with nominal water cooling parameters has been included. The input $q_{||}$ is maintained for a fixed duration (2.5 s) to study the melt dynamics. The incoming heat flux is applied uniformly along the full poloidal extent of the MB (12 mm).

Sample results are shown in Fig. 10, giving the time evolution of the peak temperature and the maximum melt depth (Fig. 10a) on the misaligned edge, together with the top surface profile in the vicinity of the LE at the end of the 2.5 s heating duration (Fig. 10b). At $q_{||} = 250\ MW\,m^{-2}$, corresponding to $q_{\perp} \sim 15.3\ MW\,m^{-2}$ on the top surface, melting of the 0.3 mm misaligned edge begins at 0.5 s. The maximum melt depth peaks at 270 μm, thereafter decreasing until the melt region effectively re-solidifies. This is a result of the melt motion which produces an effective chamfering of the LE, reducing the surface power flux density. This effect is not seen in the JET misaligned lamella melting experiment since the very deep misalignment (~1 mm) ensures that there is always a large surface area of material approximately perpendicular to the magnetic field lines and so erosion continues unabated into the lamella bulk.

During the period over which the edge melts, thermionic emission occurs as usual (at a level of $\sim 300\ Acm^{-2}$), driving a poloidal $\mathbf{j} \times \mathbf{B}$ melt motion with velocities up to $100\ cm\,s^{-1}$ (estimated to be insufficient to drive droplet splashing). This is combined with a toroidal motion of several cms^{-1} due to the gradient of surface tension in the melt region. The surface topology in the vicinity of the LE at $t = 1.5$ s (near the end of the melt duration) is presented in Fig. 10b, showing extremely high levels of undesirable material accumulation (up to 1.4 mm) at the toroidal gap edge and a complex surface relief. This is not, however, a large quantity of material per se, since, as shown in Fig. 10, the melt occurs only over a toroidal extent roughly equal to the height of the misaligned edge (300–400 μm). This is, of course, the difference between the melt motion simulation and the stationary FE calculations of Fig. 6. Assuming, as shown in Fig. 10, that a volume of only $\sim 0.3 \times 0.3 \times 12\ mm^3$ melts and is swept away from the melt zone, and that this were to happen at ~2000 misaligned MBs in the strike point vicinity (see Section 3.3), the total amount of material moved constitutes only ~41 g of W. The consequences of debris on the scale of the accumulated material shown in Fig. 10 detaching and being swept into the divertor plasma have not yet been assessed, though dedicated studies on ASDEX-Upgrade [48] and results from the JET misaligned lamella experiment [14] suggest that the perturbation to plasma operation may not be significant.

Additional simulations have been performed in which a poloidally neighbouring MB is also included (gap width 0.4 mm) without radial misalignment, but subject to the same $q_{||} = 250\ MW\,m^{-2}$. The poloidal melt motion occurs as before, with material piling up across the gap and re-solidifying on contact with the neighbouring edge (which remains below melting by virtue of the lack of misalignment). The result is clear gap bridging, at least over a toroidally very thin region (~0.5 mm). The fate of such melted material in terms of response to subsequent plasma exposure is an obvious question, as is the continued evolution of the eroded LE (which has been seen experimental under pulsed loading – Section 3.2). The latter can be addressed by further MEMOS-3D simulations. These have not yet been performed, though a simulation has been run in which a simple chamfered poloidal gap edge is assumed on a radially misaligned, unshaped MB. The chamfering is at 45° across the extent of the LE (0.3 mm). As expected, 30% higher heat fluxes (1/cos(45)) are now required to melt the edge ($q_{||} = 325\ MW\,m^{-2}$ cf. $250\ MW\,m^{-2}$ for the straight edge) and the resulting melt pool depth reaches a maximum of only ~125 μm. At first sight, this appears in

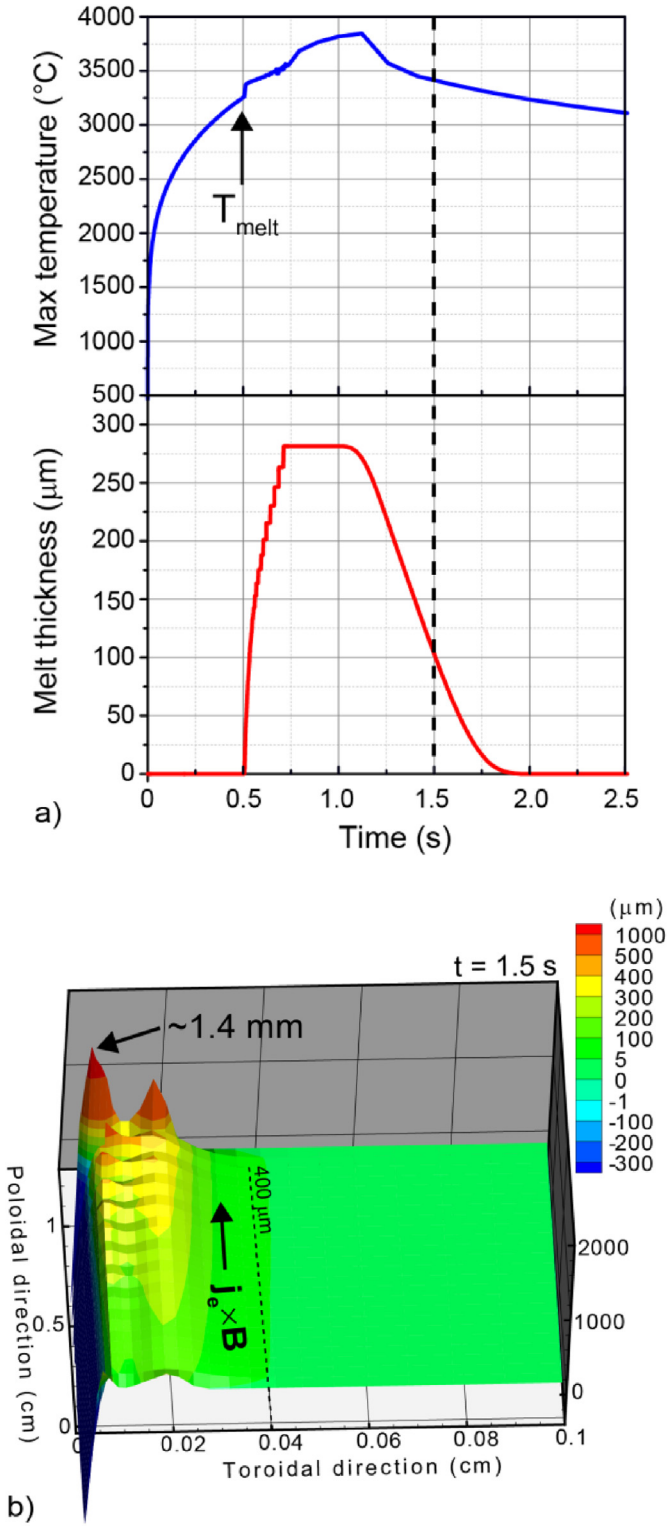

Fig. 10. MEMOS-3D simulation of a slow transient ($q_{||} = 250$ MW m^{-2}) melt event on an unshaped, misaligned ($d = 0.3$ mm) ITER inner target monoblock. (a) Time variation of peak temperature and melt thickness. (b) Surface erosion profile at $t = 1.5$ s (dashed vertical line in (a)) at the end of melting. Note the compressed scale on the ordinate. The heat flux is applied uniformly along the left hand poloidal edge to a depth of 0.3 mm (geometrical approximation with impact angle 3.7°).

contradiction to the Pilot-PSI results with a 0.3 mm misaligned edge reported in Section 3.2 (see also Fig. 8a), where multiple ELM-like heat pulses were observed to continuously erode into the bulk of the misaligned block. The difference is that whilst in the MEMOS-3D calculations for the ITER MB, $q_{||}$ was chosen always to be just sufficient for melting onset. In contrast, in the Pilot-PSI experiment, the ELM heat flux was always such that the exposed edge was significantly above $T_{melt,Al}$ during the transients, something which cannot be guaranteed never to happen on ITER. Further code simulations are required to study this.

It is interesting to note that 3D ion orbit studies of chamfering or rounding of toroidal gap edges show that such shaping brings no net benefit for transient loading since the act of shaping opens up gaps for a higher flux of ELM ions to reach gap surfaces which they could not otherwise access [11].

4. Discussion and conclusions

The last key decision to take for the ITER W divertor design is the need or not for tungsten MB front surface shaping. Small radial misalignments are inevitable between toroidally neighbouring components, exposing edges to intense power flux densities flowing parallel to magnetic field lines impacting at shallow angles, even if every effort will be made at the manufacturing stage to avoid them. Global tilting of the entire vertical targets magnetically shadows the much larger radial displacements from divertor cassette to cassette.

The simplest MB surface shaping to implement is a planar toroidal bevel of height just sufficient (with some margin) to protect the worst case radial misalignment (specified for the manufacturers at 0.3 mm). This option, with bevel height $h = 0.5$ mm, has been chosen for the ITER baseline design (Fig. 2b, lower). Unfortunately, however, the increased angle (1.0°) afforded by the inclusion of this bevel, added to that from the global target tilt (0.5°), increases the impact angle for plasma thermal fluxes on the MB surface and hence the power flux density compared with a perfectly cylindrical system. It is the trade-off between the increased power flux density, which has implications for both steady state and transient power handling, and the protection against melting of protruding edges, which is at the heart of a decision as to whether or not MB surface shaping should be applied.

An experiment at JET in 2013, devised primarily to study the physics of ELM-induced edge melting in support of the ITER divertor design, was extremely successful in demonstrating for the first time in a tokamak how transient melting could lead to heavy erosion and large scale melt motion when a deliberately misaligned edge was exposed to intense power flux densities flowing parallel to the magnetic field in the divertor strike point region during ELMs. Analysis of the experiment, however, revealed discrepancies in the parallel power loading required to explain the experimentally measured surface temperatures on the top surface of the misaligned component, casting doubt on the understanding of plasma interaction at glancing incidence. As a result, a multi-device effort, with the participation of the ASDEX-Upgrade, COMPASS, DIII-D, JET and KSTAR tokamaks and the Pilot-PSI and Magnum-PSI linear devices, was launched within the ITPA Divertor and SOL Topical Group to investigate both leading edge power loading and to further study melt dynamics.

With regard to non-transient edge power loading (i.e. in the absence of ELMs), a very detailed series of experiments on COMPASS [17] and Magnum-PSI [21] found no deviations from power loading according to the optical (geometrical) approximation. First experiments performed on KSTAR [16] and DIII-D [18] reached the same conclusion. A second experiment on JET with a modified target element (a sloped surface in place of a perpendicular misaligned edge), improved diagnostics and analysis methods concludes that

geometric loading is now consistent with measurements, for both L- and H-mode. Moreover, application of the improved analysis techniques developed for this second experiment finds, retrospectively, that the original discrepancies in the first, misaligned edge experiment, are now explicable and do not originate from any new physics of edge power loading [23,24]. A replica of the original JET experiment, performed on ASDEX-Upgrade, also concludes that the OA applies in both L- and H-mode [19].

Meanwhile, an exhaustive comparison between the 3D ion orbit calculations which have been used to study the proposed ITER MB shaping solution and more complex (and CPU intensive) PIC simulations accounting self-consistently for local electric fields, has shown that the simpler orbit approach is an excellent approximation to the local power loading in the case of both stationary and ELM-driven power loads [12]. In the former case, ion orbits are sufficiently small, particularly on ITER, that the assumption of geometric loading is valid. Even in some of the ITPA experiments with low enough magnetic field to produce ion orbits on the scale or larger than the dimension of the radially misaligned edge, "Larmor smoothing" effects, though predicted to occur in the LE vicinity, cannot in general be experimentally discerned owing to the small spatial scales involved. For the ELMs, where ion energies, and hence orbits, are higher, similar conclusions apply thus far, though the analysis of data from KSTAR and DIII-D on detailed ELM leading edge power loading is awaited at the time of writing.

Concerning edge melting, the quantitative agreement obtained with the MEMOS-3D melt code in comparison with the ELM-driven gross erosion/melt motion found in the original JET misaligned edge experiment is extremely encouraging with respect to the validity of calculations being made for ITER with the same code. Replication of this same melt motion in a separate experiment in identical geometry on ASDEX-Upgrade [19], reinforces the conclusions regarding the key physics at work. The dominant drive for the melt motion is identified as the $\mathbf{j} \times \mathbf{B}$ force due to intense thermionic emission from the melted surface, with the dynamics intimately linked to the geometry of the situation. This latter aspect, including the structure of electric fields and the trajectories of the emitted electrons in the leading edge vicinity, is an area for further study, both experimental and theoretical, given the rather crude treatment currently included in MEMOS-3D. In particular, better understanding of the global return current paths in the system, the dynamics of electron return to the melt surface and a better description of the virtual cathode forming due to space charge under transient conditions would help in improving model development. More work is also required to examine the current pathways inside the material in the vicinity of the melted surface.

The outcome thus far of the multi-device ITPA study, together with theoretical studies of edge power loading, therefore concludes that geometrical, or optical power loading can be assumed to zero order when comparing misaligned shaped or unshaped MBs to stationary and ELM transient heat fluxes from the point of view of the "global" response. That is, neglecting the fine details of tiny "optical hotspots" appearing during stationary operation or very localized toroidal and poloidal gap edge melting during ELMs which are only revealed when 3D ion orbits are fully accounted for [10,11].

Under these conditions, thermal calculations for stationary heat fluxes conclude in favour of toroidal shaping from the point of view both of the avoidance of continuous edge overheating during normal operation and of severe edge melting in the case of slow transient situations when divertor heat flux control may be lost. Simulations of the melt motion which would occur in this case if MBs were left unshaped predict rapid accumulation of melted material and potential toroidal gap bridging, though calculations have not yet been performed to study the subsequent behaviour once the bulk of the LE has been removed. Nor can the fate of the melted material be quantitatively predicted by simulation. Experimentally, there is evidence that erosion of the melted edge continues into the bulk of the material if the heat flux persists at high enough levels, even for the relatively low worst case misalignments expected in the ITER divertor.

From the point of view of melting, if $\mathbf{j} \times \mathbf{B}$ forces are assumed as the main drivers, then it probably matters little whether the melting occurs in a single "slow transient" event, or as the result of accumulated ELM driven events. Even though chamfering of misaligned poloidal gaps can increase the threshold for melting during stationary (inter-ELM) loading, the gain will be of no consequence for insufficiently controlled ELMs, where energy densities are transiently much higher and take the edge far above melting. As a result, the principle gain from toroidal bevelling (subject to ELMs being appropriately managed in terms of plasma energy loss) is the prevention of material accumulation possibly leading to toroidal gap bridging across poloidally neighbouring MBs (which has consequences for current flow between blocks during disruptions) and the danger of continued erosion into the bulk of the MBs once the initial LE has been removed. If toroidal bevelling is applied, but ELMs are still sufficiently energetic to melt the top surface (unlikely before the burning plasma phase of ITER operation [9]), then the absence of a sharp edge leads, if the melt simulations are correct, to greatly reduced material accumulation. This conclusion applies also of course to the top surface of an unshaped MB, but with the difference that much more serious melting will also occur on the poloidal gap edge, even in the absence of radial misalignment. It is perhaps worth making the somewhat obvious statement that if the accumulated surface topological damage approaches or exceeds the bevel height, then the shaping can no longer be considered effective. This kind of approximate criterion can be used to fix a crude "budget" for the number of allowed transient events at given energy density in ITER, in particular for disruptions [49].

On the basis of the results shown here, *it is therefore concluded that poloidal gap edge protection should be provided on the ITER divertor monoblocks in the high heat flux areas of the vertical targets.* A simple toroidal bevel is the easiest solution to implement technologically, though more sophisticated 3D ion orbit simulations demonstrate that this does not completely eliminate the risk of ELM-driven melting on poloidal gaps, and offers no protection with respect to toroidal gap edge melting during ELMs, which always occurs first, before top surface melting [10,11].

Acknowledgements

The views and opinions expressed herein do not necessarily reflect those of the ITER Organization and of the European Commission. ITER is the nuclear facility INB 174. Portions of this work were performed under the auspices of the U.S. Department of Energy by Lawrence Livermore National Laboratory under Contract DE-AC52-07NA27344. This material is based upon work supported by the U.S. Department of Energy, Office of Science, Office of Fusion Energy Sciences.

References

[1] M. Merola et al., Fusion Eng. Des. 89 (2014) 890.
[2] R.A. Pitts, et al., J. Nucl. Mater. 438 (2013) S48.
[3] A.S. Kukushkin, et al., Fusion Eng. Des. 86 (2011) 2865.
[4] A.S. Kukushkin, et al., Nucl. Fusion 49 (2009) 075008.
[5] T. Hirai, et al., Phys. Scr. (2014) 014006 T159.
[6] T. Hirai, et al., J. Nucl. Mater. 463 (2015) 1248.
[7] S. Carpentier, et al., Phys. Scr. (2014) 014002 T159.
[8] T. Hirai, et al., Fusion Eng. Des. 88 (2013) 1798.
[9] A. Loarte, Nucl. Fusion 54 (2014) 033007.
[10] J.P. Gunn, et al., Surface Heat Loads on the ITER Divertor Vertical Targets, Nucl. Fusion 57 (2017) 046025.
[11] J.P. Gunn, et al., Ion orbit modelling of ELM heat loads on ITER divertor vertical targets, Nucl. Mat. Energy (2017) in press.

[12] M. Komm, et al., Particle-in-cell simulations of heat loads on ITER divertor monoblocks during steady state and transient plasma loading conditions, Nucl. Fusion (2016) To be submitted.
[13] J.W. Coenen, et al., J. Nucl. Mater. 463 (2015) 78.
[14] J.W. Coenen, et al., Nucl. Fusion 55 (2015) 023010.
[15] R. Dejarnac, et al., Nucl. Fusion 54 (2014) 123011.
[16] S.H. Hong et al., "Tungsten Leading Edge Heat Loads in the KSTAR Divertor", Accepted for publication in Nuclear Materials and Energy.
[17] R. Dejarnac et al., "Power deposition on misaligned edges in COMPASS", Nucl. Mat. Energy, in press.
[18] R.E. Nygren et al., Bulletin of the American Physical Society Vol. 60 No. 19 (2015). See http://meetings.aps.org/link/BAPS.2015.DPP.PP12.116.
[19] K. Krieger et al., "Investigation of repetitive transient tungsten melting by ELMs in ASDEX Upgrade", Nucl. Fusion. To be submitted.
[20] R Dejarnac, et al., J. Nucl. Mater. 415 (2011) S977.
[21] T.W. Morgan et al., "Power deposition on misaligned, castellated tungsten blocks in the Magnum-PSI and Pilot-PSI linear devices", Nucl. Fusion. Submitted to.
[22] Abaqus 6.13, Abaqus Documentation, Dassault Systèmes Simulia Corp, Providence, RI, USA, 2013.
[23] D. Igelsias et al., "An improved model for the accurate calculation of parallel heat fluxes at the JET bulk tungsten outer divertor", Nucl. Fusion. To be submitted.
[24] Y. Corre et al., "Thermal analysis of transient tungsten melting experiments at JET", Nucl. Fusion. Submitted.
[25] M.G. Dunne, Nucl. Fusion 57 (2017) 025002.
[26] H.D. Pacher, et al., J. Nucl. Mater. 463 (2015) 591.
[27] E. Kaveeva et al., "SOLPS-ITER modelling of the ITER edge plasma with drifts and curents", Nucl. Mater. Energy. Submitted.
[28] S. Panayotis, et al., Thermo-mechanical analysis of ITER divertor tungsten monoblocks under high heat flux loadings, Fusion Eng. Des. (2016) Submitted for publication.
[29] G. Pintsuk, Tungsten as a plasma-facing material, Reference Module Mater. Sci. Mater. Eng., Compr. Nucl. Mater. 4 (2012) 551–581.
[30] Ph. Mertens, et al., Phys. Scr. (2009) 014032 T138.
[31] I. Smid, et al., J. Nucl. Mater. (1998) 258–263 160.
[32] S. Panayotis et al., "Self-castellation of tungsten monoblock under high heat flux loading and impact of material properties", Nucl. Mater. Energy, in press.
[33] B. Bazylev, et al., J. Nucl. Mater. (2009) 390–391 810.
[34] J.W. Coenen, et al., Nucl. Fusion 51 (2011) 083008.
[35] G. Sergienko, et al., Phys. Scr. T128 (2007) 81.
[36] O.W. Richardson, Science 38 (1913) 57.
[37] S. Dushman, General Electric Rev. 18 (1916) 156.
[38] I. Langmuir, Phys. Rev. 2 (1913) 450.
[39] C.D. Child, Phys. Rev. 32 (1911) 492.
[40] C. Guillemaut, et al., Plasma Phys. Control. Fusion 57 (2015) 085006.
[41] S. Takamura, et al., Contrib. Plasma Phys 44 (2004) 126.
[42] S. Bardin, et al., in: The Effect of Misalignment at Grazing Angle of Incidence for ELM-Like Plasma Loading, Presented at 22nd PSI Conference, Rome, Italy, May 30–June 3, 2016.
[43] C. Costin, et al., Plasma Sources Sci. Technol. 25 (2016) 025023.
[44] G. De Temmerman, et al., Nucl. Fusion 53 (2013) 023008.
[45] G. Sergienko, et al., Phys. Scr. (2014) 014041 T159.
[46] T. Eich et al., "ELM divertor heat load scaling to ITER with data from JET, MAST and ASDEX Upgrade", Nucl. Mater. Energy, Submitted.
[47] Yu. Igitkhnov, G. Janeschitz, J. Nucl. Mater. 290–293 (2001) 99.
[48] K. Krieger, et al., J. Nucl. Mater. 415 (2011) S297.
[49] M. Lehnen, et al., Plasma disruption management in ITER, in: 26th IAEA Fusion Energy Conference, 17–22 October, Kyoto, Japan, 2016 paper EX/P6-39.